Available online at www.sciencedirect.com
ScienceDirect
International Journal of Mass Spectrometry 258 (2006) 30–36
International Journal of Mass Spectrometry
www.elsevier.com/locate/ijms

An experimental study of nanoparticle focusing with aerodynamic lenses

Xiaoliang Wang [1], Peter H. McMurry *

Department of Mechanical Engineering, University of Minnesota, 111 Church Street SE, MN 55455, USA

Received 21 March 2006; received in revised form 13 June 2006; accepted 13 June 2006
Available online 25 July 2006

Abstract

High sampling efficiencies of analyte ions, molecules or particles are needed to maximize the sensitivity of mass spectrometers. "Ion funnels", which utilize electrodynamic focusing, have been shown to effectively focus ions with mass-to-charge ratio (m/z) ranging from ~100 to 5000. Focusing efficiencies of ion funnels drop for higher m/z values because very high voltages are needed to overcome the particle inertia. Conventional "aerodynamic lenses" utilize inertia to focus down to 25 nm in diameter (~5 MDa); to date, Brownian diffusion has prevented the effective focusing of particles smaller than this. We recently reported a design procedure that should, in principle, extend focusing with aerodynamic lenses to particles as small as 3 nm (~10 kDa), thereby bridging the gap between the ion funnel and the conventional aerodynamic lenses. In this paper, we report for the first time experimental results for the performance of these new "nanolenses". Measurements were done using spherical oil droplets, proteins, and sodium chloride particles ranging in size from 3 to 30 nm diameter. We found that particle transport efficiencies from atmospheric pressure to vacuum through the aerodynamic lens system were greater than 80% for 10–30 nm particles, and greater than 50% for a ~3.8 nm protein (Lysozyme from chicken egg white, molecular weight 14.3 kDa). Particle beam diameters were about a factor of two greater than predicted by our numerical simulations, but provide clear evidence that the nanolenses effectively focus all three particle types.

Keywords: Aerodynamic lens; Focusing; Particle beam; Transmission efficiency; Electrospray; Nanoparticle

1. Introduction

Mass spectrometers are used in a wide variety of applications, including the analysis of biological molecules and environment pollutants. Analytes are sometimes transported from atmospheric pressure into the high vacuum mass analyzer region, and instrument sensitivity depends on the transport efficiencies. Traditionally, capillaries, sampling cones or orifices are used as inlets to the first differential pumping stage of mass spectrometers. Charged particles expand from these inlets due to gas expansion and space charge repulsion. Thus only a small fraction of the analyte typically passes through the small apertures (skimmers) that separate different pumping stages. It has been reported that when ions are produced by electrospray at atmospheric pressure, only 1 in 10^2 to 10^6 particles are ultimately detected after the ions are expanded to low pressure and separated by mass [1–3].

Richard Smith and co-workers developed the "ion funnel" to facilitate efficient ion transport [2,4–8]. This device uses electrodynamic forces generated by radiofrequency (RF) fields using a stack of ring electrodes with decreasing internal diameters. A DC potential is used to drive ions toward the exit. An optimized configuration enables near 100% transmission efficiency in the mass-to-charge ratio (m/z) range of ~100–5000 [8]. The upper limit of m/z is imposed mainly by the ion/particle inertia and the breakdown of the RF field at higher amplitudes.

Aerodynamic lenses [9,10] have been widely used in aerosol mass spectrometers to focus particles into collimated beams and efficiently deliver them into the mass analyzing region [11–20]. In contrast to the "ion funnel", which uses an oscillating electrodynamic force to focus particles, aerodynamic lenses focus particles by causing them to deviate from gas streamlines due to their inertia as the carrier gas passes through a sequence of contractions and expansions. In this manner aerodynamic lenses focus particles into a tightly collimated beam, which is then delivered through an accelerating nozzle to the first stage of the differential pumping chamber. The original lens system

* Corresponding author at: Particle Technology Laboratory, Department of Mechanical Engineering, University of Minnesota, 111 Church Street SE, MN 55455, USA. Tel.: +1 612 624 2817; fax: +1 612 626 1854.
E-mail addresses: wxl@me.umn.edu (X. Wang), mcmurry@me.umn.edu (P.H. McMurry).
[1] Present address: TSI Inc., 500 Cardigan Road, Shoreview, MN 55126, USA.

1387-3806/$ – see front matter © 2006 Elsevier B.V. All rights reserved.
doi:10.1016/j.ijms.2006.06.008

designed by Liu et al. [9,10] samples aerosol from atmospheric pressure through a pressure limiting orifice into the lenses operating at ~200 Pa. Typically a series of five lenses progressively focus spherical particles covering a range of about a factor of ten in particle diameter (e.g., ~25–250 nm), or 1000 in mass. The beauty of an aerodynamic lens system is that it uses simple mechanical parts and focuses a wide range particle sizes. Furthermore, it does not require the particles to be charged. However, space charge might degrade the beam quality if particles are highly charged.

There is an interest in developing mass spectrometers that efficiently measure high mass analytes (such as proteins and other large biomolecules), and in developing aerosol instrumentation that can detect very small particles (such as are formed in the atmosphere by homogeneous nucleation). Aerodynamic lenses have been successfully used to focus particles from tens of nanometers to several micrometers [21]. However, it remains a great challenge to focus particles smaller than 20 nm (~2.5 MDa) aerodynamically due to their low inertia and high diffusivity. On the other hand, macromolecues with *m*/*z* over ~5000 require such high amplitude of RF voltages in the "ion funnel" that the gas will break down, which imposes a practical upper limit on this approach [8]. A focusing device that performs well for particles in the 3–30 nm diameter range (~10 kDa to 10 MDa) would help to enable such measurements. In an effort to fill this gap, Wang et al. [22,23] developed a systematic procedure to design aerodynamic lens systems for nanoparticles. They recognized that lighter carrier gases such as helium are preferred in focusing small particles, and they optimized the operating conditions and lens dimensions so as to arrive at a design that effectively focuses 3–30 nm spherical particles of unit density. They carried out detailed numerical simulations of flow and particle transport through the lens system and demonstrated in principle the effectiveness of this focusing device.

This paper describes the first measurements of nanoparticle focusing with an aerodynamic lens system that was optimally designed for that purpose [23]. Measurements were done with singly charged oil, sodium chloride and protein particles ranging in mobility diameter from 3 to 30 nm (*m*/*z* ~10,000–10,000,000). The particle transmission efficiency through the lens system and the width of the particle beam were measured. The results of our measurements are compared with numerical simulations [23] and an empirical model [21].

2. Experimental method

The experimental setup used to study nanoparticle focusing is shown in Fig. 1. Particles were generated by an aerosol generator, which is either a tube furnace or an electrospray, and then charged by a unipolar charger [24]. A nanoparticle differential mobility analyzer (TSI 3085 Nano-DMA) was used to select charged particles within a narrow range of electric mobility [25,26]. The concentration of these singly charged "monodisperse" particles exiting the DMA was measured by a Faraday cup electrometer (FCE) [27]. In parallel, a fraction of the aerosol flow went through a critical orifice which reduced the pressure from atmospheric pressure to the lens operating pressure (~530 Pa). Particles were focused into a tight beam as they passed through the aerodynamic lens system and were delivered into a vacuum chamber. The particle flux and beam diameter were measured by a beam stop and a copper plate connected to an electrometer. In this section the experimental method is described.

2.1. Nanoparticle generation

Particles in the size range of 3–30 nm were generated from three different materials: sodium chloride (NaCl), vacuum pump oil (Santovac® 5P ultra) and seven proteins. Sodium chloride particles are used to test focusing performance of the nanoparticle lens system for nonspherical (near cubic) solid particles. The Santovac® 5P ultra vacuum pump oil has a density of 1.2 g/cm^3 and a very low vapor pressure (5.3×10^{-8} Pa at 25 °C). At this vapor pressure, oil droplets as small as 4.5 nm will not evaporate significantly during timescales pertinent to our measurements [28]. These particles were used to test the focusing performance for spherical liquid particles. Proteins are frequently analyzed by mass spectrometry. We evaluated the transport efficiency and beam width of selected aerosolized protein particles as a test of the nanoparticle lens system for one possible application.

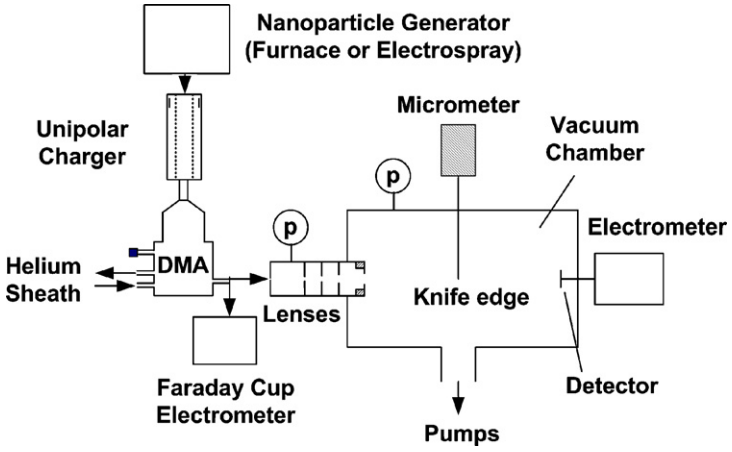

Fig. 1. Experimental setup for the nanoparticle lens system evaluation.

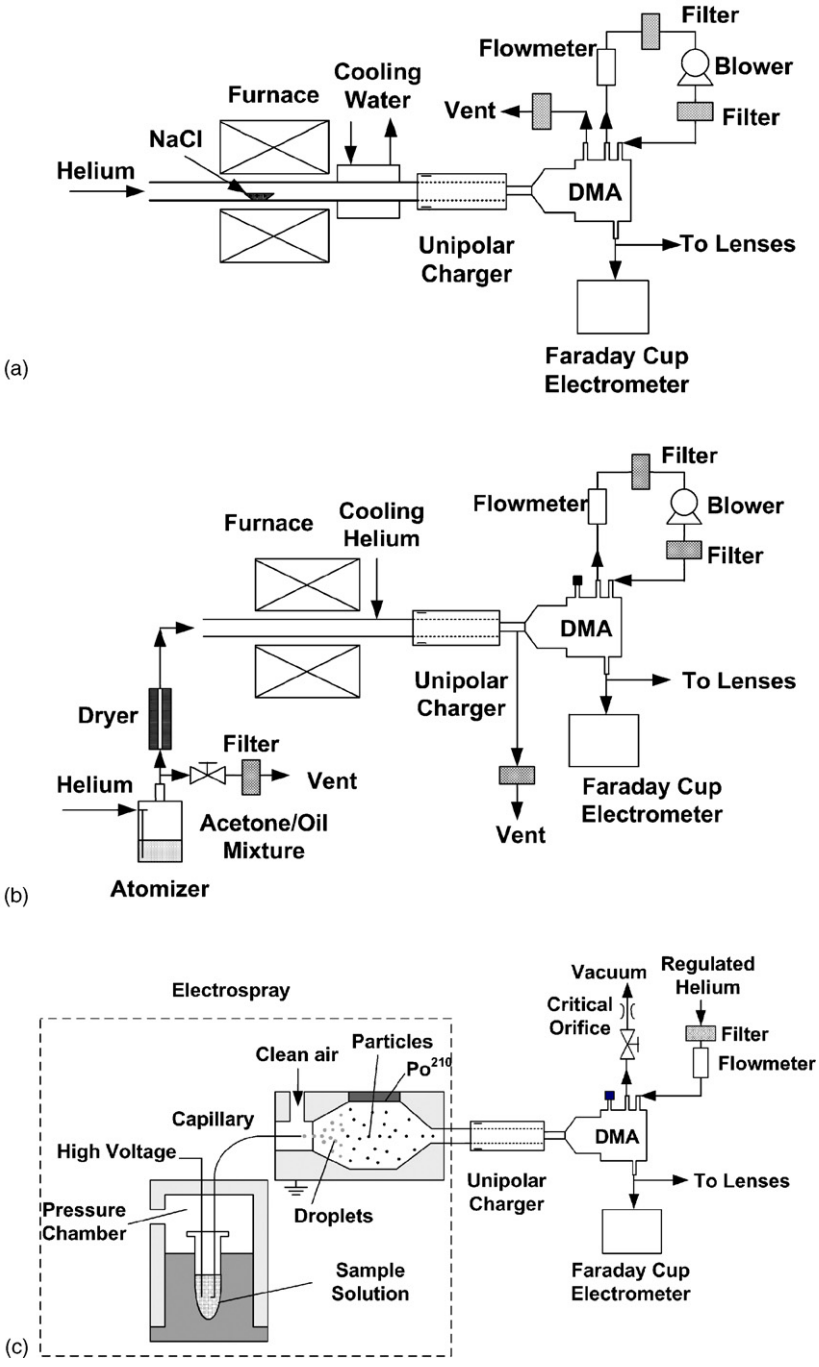

Fig. 2. Experimental setup for generating monodisperse (a) NaCl particles, (b) oil particles (15–30 nm), (c) oil particles (4.5–14 nm) and proteins (3.8–14.2 nm).

Sodium chloride particles were generated using the evaporation–condensation method [29]. As shown in Fig. 2a, NaCl powder contained in a ceramic boat was heated in a tube furnace (Lindberg/Blue M). A constant helium flowrate of 2.5 l/min carried the NaCl vapour away from furnace. The flow was cooled by 5 °C chilled water at the exit of the furnace. Ultrafine NaCl particles were generated by nucleation and condensation when the NaCl vapor became supersaturated. The peak of the particle size distribution can be adjusted from about 30–3 nm by adjusting the furnace temperature from about 560 to 460 °C. A unipolar charger similar to that described by Chen and Pui [24] was used to increase the fraction of negatively charged nanoparticles, and thus to increase the DMA classified "monodisperse" particle concentration. The DMA sheath flow was maintained at 15 l/min and was recirculated to avoid wasting helium. A polydisperse aerosol flowrate of 2.5 l/min entered the DMA, and 0.731 l/min of this exited the DMA through the bypass port. The monodisperse aerosol flowrate out of the DMA was split between the Faraday cup electrometer (1.681 l/min) and the aerodynamic lens system (88 cm^3/min).

Two approaches were used to generate the vacuum pump oil particles. Particles in the 10–30 nm size range were generated

using the evaporation–condensation method [30]. As shown in Fig. 2b, the oil was dissolved in acetone to make a 0.1% (volume) solution and aerosolized using a Collison atomizer. The acetone rapidly evaporated from the particles and was adsorbed by activated carbon in the "dryer". Oil droplets were then fed into the furnace, which was maintained at a temperature of 250 °C, where they evaporated. The oil vapor exiting the furnace was cooled by filtered helium, causing the oil to nucleate. The peak of particle size distribution can be changed from 30 to 15 nm by adjusting the flowrate of the cooling helium from 0 to 2.5 l/min. Although this method can generate very high concentrations of oil particles, we were not successful in obtaining repeatable results. Furthermore, no operating conditions were found to achieve high enough concentrations for particles smaller than 10 nm.

We used a TSI Model 3480 electrospray [31,32] as shown in Fig. 2c to generate oil particles in the size range of 4.5–14 nm. The sample solution was stored in a pressurized vial (25.5 kPa). A capillary with 25 μm inner diameter and a high voltage platinum wire (2.0–2.3 kV) were immersed in the solution. The pressure difference across the capillary pushed the solution through the capillary at a flowrate of ~60 nl/min. The electric field between the exit of the capillary and the grounded orifice plate in the spray chamber created a fine cone jet which broke up into droplets. The droplets had an average size of about 150 nm [33,34]. The highly charged droplets were swept by clean air and neutralized by bipolar ions generated by a radioactive Po^{210} source to minimize electrostatic losses. The solvent evaporated before the aerosol exited the electrospray. The buffer solution used for spraying oil particles was made by dissolving 308 mg ammonium acetate in 43.7 ml pure ethanol and then adding 6.3 ml toluene. Oil particles in the 4.5–14 nm range and having very narrow size distributions (geometric standard deviation 1.11–1.23) were obtained by using oil/buffer solutions with concentrations from 0.0005 to 0.02%. Particles exiting the electrospray were again charged with the unipolar charger and classified by the Nano-DMA.

Because helium breaks down at a lower voltage than air, it cannot be used directly as the working gas in the electrospray. Therefore, the Nano-DMA here served not only as a mobility classifier, but also as a gas converter [35] which changed the aerosol carrier gas from air to helium. Due to the mixing of air and helium, the DMA sheath flow was not recirculated when nanoparticles were produced using the electrospray. The sheath flow rate was maintained at 16.03 l/min by a critical orifice and a valve and monitored by a laminar flow meter. Particles contained in the 1.534 l/min inlet air stream migrate through the 16.03 l/min helium sheath air. Due to the large helium to air ratio, only a very small fraction of the air will exit the DMA with the classified particles. Earlier studies reported that using different gases for DMA aerosol inlet and sheath flows causes a small sizing error [35,36]. When we scanned the DMA voltage while monitoring the electrometer current we found that the highest current occurred at about the same voltage as would have been expected if the polydisperse aerosol gas was helium rather than air. Therefore we simply used this voltage to infer the classified particle mobility size.

Table 1
Molecular weight of proteins used in this experiment and their measured electrical mobility diameters

Protein	M (Da)	d_p (nm)
Ubiquitin (bovine), dimer	17130	4.6
Lysozyme from chicken egg white	14305	3.8
Trypsin from bovine pancreas	23853	5.3
Albumin from chicken egg white	44564	6.3
Albumin from chicken egg white, trimer	133692	8.7
Albumin from bovine serum	66398	6.73
Albumin from bovine serum, dimer	132797	8.2
IgG from bovine serum	148850	8.74
IgG from bovine serum, dimer	297700	10.62
Thyroglobulin from bovine thyroid	660000	14.2

The setup for protein particle generation and beam evaluation is the same as the one used for oil particles as shown Fig. 2c. However, a capillary with inner diameter of 30 μm was used to increase the concentration of the sprayed protein ions. The buffer used for electrospraying protein was 20 mM ammonium acetate aqueous solution with pH adjusted to 8.5 [32]. The solution concentrations of proteins were optimized to provide highest output of monomer or dimer particle concentrations. The molecular weight (M) [37] and measured electrical mobility diameters (d_p) of the seven proteins used in this experiment are listed in Table 1. Bacher et al. [37] measured the mobility diameter of a wide range of biomolecules with a method similar to ours. Their measurements and ours are both plotted in Fig. 3. Note that a power law fitting with an index of about three fits the experimental data points very well, suggesting that when aerosolized, the proteins are compact. If the proteins are assumed to be spherical, then the effective densities of the proteins can be calculated from the ratio of the protein molecular weight to the protein volume. We have used two approaches to calculate the volume. First, the volume was calculated assuming that the protein diameter equals the mobility equivalent diameter. In this case the protein density varied from 0.51 to 0.83 g/cm^3. Second, the volume was calculated using the "mass diameter", which accounts for the size of carrier gas molecules on mobility [38]. In this case the effective densities range from 0.73 to 0.96 g/cm^3

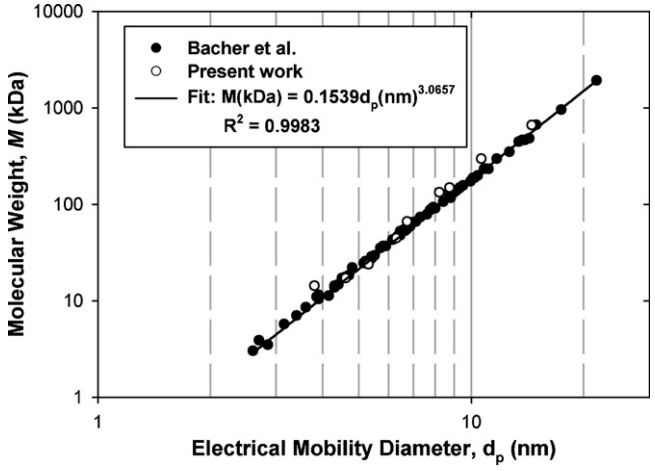

Fig. 3. Electrical mobility diameter vs. molecular weight of proteins.

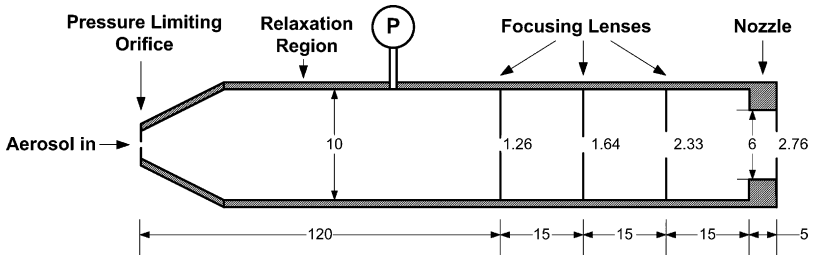

Fig. 4. Schematic of the nanoparticle aerodynamic lens system. All dimensions are in millimeters.

(with one outlier at 1.38 g/cm^3). These values are somewhat below reported protein crystal densities, which range from 1.22 to 1.47 g/cm^3 [39–41]. Possible explanations for the discrepancy include hydration or nonspherical shape, both of which would lead to measured mobility sizes that are larger than the spherical equivalent diameters of the unhydrated proteins [38,42].

2.2. Aerodynamic lens inlet for nanoparticles

The nanoparticle aerodynamic lens system shown in Fig. 4 is the same as the one described in our previous work [23]. It was designed to focus 3 nm spherical particles of unit density. A critical orifice (O'keefe, No. 7 sapphire orifice, aperture diameter 71 μm) limits the aerosol flowrate (helium) into the lens system at 88 cm^3/min. The pressure drops from atmosphere pressure to about 530 Pa (predicted by simulation and confirmed by measurement) after the critical orifice. The aerosol slows down in the "relaxation region" before it reaches the first focusing lens. Particles are progressively focused into a narrow beam by three lenses in this focusing inlet. The aperture diameters of the three lenses are 1.26, 1.64 and 2.33 mm in sequence and the spacers between lenses are 15 mm in length and 10 mm in diameter. Finally particles are accelerated through a step nozzle, which is known to produce a low divergence expansion into a vacuum [10].

We carried out detailed numerical simulations of particle motion through this lens system [23]. It was found that the transport efficiencies of 2–40 nm spherical particles are 56–99%, with diffusional losses dominant for particles smaller than 10 nm and impaction losses dominant for particles larger than 40 nm. The simulations also demonstrated that for spherical particles, this lens system can achieve beam widths as narrow as the limits imposed by Brownian motion assuming that particles are all on the centreline at the exit from the nozzle [9].

2.3. Particle beam evaluation

Particle transport efficiency and beam width are measured in this experiment. The particle beam was measured in the vacuum chamber downstream of the aerodynamic lens system. The pressure in the chamber was maintained around 0.7 Pa with a 20 l/s (helium) turbomolecular pump (Pfeiffer TMH 260) backed by a 35 m^3/h mechanical pump (Alcatel 2033). This vacuum ensures that 1.5 nm particles of unit density will have a sufficiently long stopping distance to reach the detector before being drawn to the pumps.

The method for measuring particle beam characteristics is similar to that described by Liu et al. [10]. The singly charged particles classified by the DMA were collected on a detector located 180 mm downstream of the exit of the accelerating nozzle, and the current delivered by the particle beam (I_{beam}) was measured using a sensitive electrometer (Keithley 624, noise level $\sim 10^{-17}$ A). The detector was a copper disk with a diameter of 3.8 cm, and was connected to the electrometer with a low-noise vacuum feed through. A knife edge particle beam stop was mounted 71 mm downstream of the nozzle exit to probe the particle beam width.

Particle transport efficiency (η_t) through the pressure limiting orifice and the nanoparticle lens system can be calculated from:

$$\eta_t = \frac{I_{beam}}{I_{ref}} \frac{Q_{ref}}{Q}, \quad (1)$$

where I_{ref} is the aerosol current measured by the Faraday cup electrometer (FCE) upstream of the lens system, Q_{ref} the volumetric flowrate through the FCE, and Q is the flowrate through the lens system.

The particle beam width was determined by moving the knife edge incrementally across the particle beam and measuring the attenuated current as a function of the beam stop position. Assuming that the radial particle beam intensity has a Gaussian distribution [10,43], the fraction of particles that is not shielded by the beam stop and arrives at the detector can be approximated by

$$I(x) = \frac{1}{2}\left[1 - \mathrm{erf}\left(\frac{x}{a_e}\right)\right] \quad (2)$$

where x is the shortest distance from the knife edge to the beam axis, I the measured current, erf the error function, and a_e is a fitting parameter that is related to the particle beam diameter by $d_B = 3.04a_e$ [10]. Here the particle beam diameter is defined as the beam width that encloses 90% of the total particle flux.

3. Results

Fig. 5(a) shows the particle transmission efficiencies through the nanoparticle lens system. The symbols show the data for the three particle materials, the dashed line is the prediction by the aerodynamic lens design tool developed by the authors [21], and the dash-dot line was obtained by numerical simulation [23]. Both the design tool prediction and simulation assume that particles are unit density spheres. The error bars on the data

points represent one standard deviation obtained from repeated measurements.

Note that the particle transport efficiencies through this lens system are very high. The efficiencies are greater than 80% for 10–30 nm particles, and greater than 50% for a ~3.8 nm protein (Lysozyme from chicken egg white, with molecular weight 14.3 kDa). For reasons that are still unclear, the proteins have the highest transport efficiencies among the three materials. However, oil and salt particles have similar efficiencies for most sizes. The prediction of the aerodynamic lens design tool agrees reasonably well with the experiments. The numerical simulation predicts higher transmission efficiencies than were observed experimentally or obtained using the design tool. This is because only 20 mm of the flow path upstream of the first lens was considered in the simulation, while in reality the distance between the critical orifice and the first lens (i.e., relaxation chamber) is 120 mm (see Fig. 4). Significant diffusional losses happen in this section because particles are not well focused there. Therefore, the numerical simulation significantly underestimated particle losses compared to the experiment.

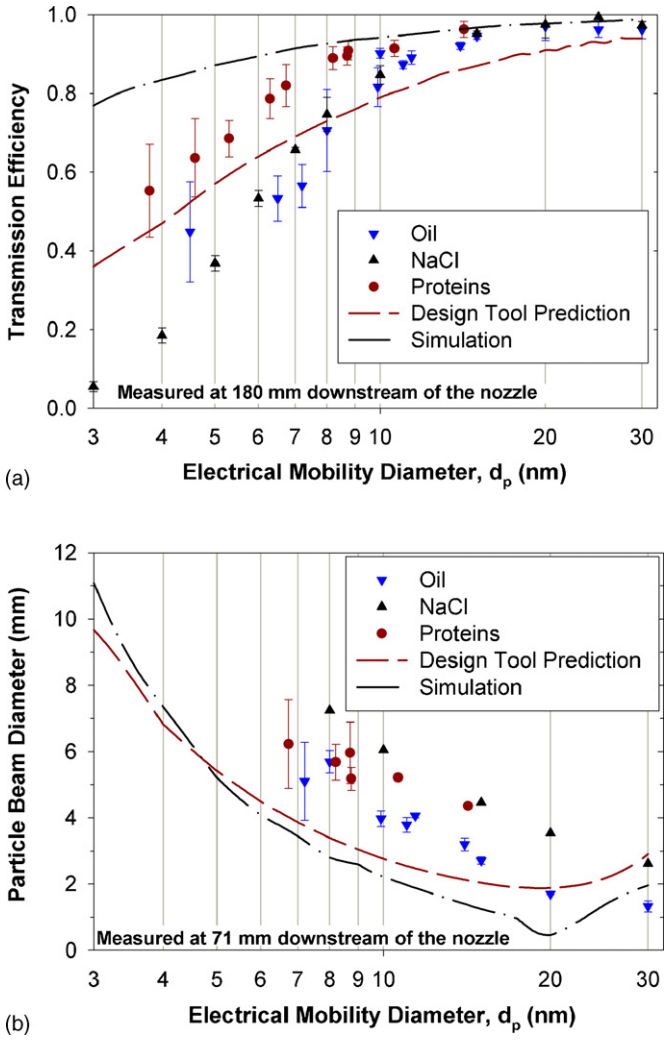

Fig. 5. Measured transmission efficiency (a) and particle beam width of oil, NaCl and protein nanoparticles downstream of the aerodynamic lens system (b). Also shown are the values predicted by the aerodynamic lens design tool and by numerical simulation, assuming that particles are neutral spheres with unit density.

Fig. 5(b) shows the particle beam diameter which encloses 90% of the total particle flux measured 71 mm downstream of the nozzle. Also shown are the predictions by the design tool and the numerical simulations. The first thing to note is that among the three particle materials, the oil particles have the smallest beam diameters. This is probably because the oil particles are perfectly spherical and have the smallest broadening effects due to aerodynamic lift forces [10]. The salt particles have the largest beam diameters. The reason is, as was explained by Liu et al. [10], that the salt particles are not ideal cubes and suffer broadening by aerodynamic lift. The beam widths of protein particles lie somewhere between the oil and salt particles. This phenomenon indicates that proteins are more spherical than salt but less than oil. The actual shape of these protein particles in the gas phase is still not known to us. The predicted particle beam widths by the design tool or by numerical simulation are systematically smaller than the experimental values. Since particles in the experiment each contain one negative charge while particles were assumed neutral in the design tool or simulation, space charge will contribute to beam broadening. However, back-of-the-envelop calculations indicate that effects of space charge on beam widths are almost negligible at concentrations pertinent to our experiment. We do not understand why the observed beam diameters are systematically greater than predicted.

Note that we measured the particle beam width 71 mm downstream of the nozzle exit. The particle beams are narrower at distances closer to the nozzle. Our numerical simulation showed that the beam diameter for 4 nm particles is less than 0.9 mm at 5 mm downstream of the nozzle [23]. This permits using small apertures of skimmers for differential pumping while maintaining high transmission efficiencies of particles.

4. Discussions and conclusions

We carried out an experimental study of nanoparticle focusing using aerodynamic lenses. Measurements were done with DMA-classified particles in the 3–30 nm diameter range for three types of materials: vacuum pump oil, sodium chloride and proteins. The particles were focused by an aerodynamic lens system designed for nanoparticles, using helium as the carrier gas. The particle transport efficiency through the aerodynamic lens and the beam width downstream of the lens system were measured. The results showed that this lens system can effectively deliver nanoparticles (3–30 nm) from atmosphere pressure to high vacuum with high transmission efficiencies and narrow beam diameters. The measured transmission efficiencies are close to values predicted by our empirical model, while the measured particle beam widths were greater than predicted.

The nanoparticle lens system fills a size gap for particle/ion focusing between the conventional aerodynamic lenses and the "ion funnel". Aerodynamic lenses offer the advantages of simplicity and a wide dynamic range in size. Particles may still be focused even if desolvation is occurring as they are being transported through the lens system. Furthermore, the particles do not need to be charged to be focused. On the other hand,

the minimum size that can be focused with aerodynamic lenses is limited by Brownian diffusion. The particle beam quality degrades quickly as particle size approaches a few nanometers (molecular weight of a few kilo Dalton). Aerodynamic lenses work best for spherical particles, and the beams are wider for nonspherical particles due to aerodynamic lift. In contrast, electrodynamic focusing is better suited for particles that are too small to be focused aerodynamically.

Acknowledgements

This work was supported by NSF (Grant No. DMI-0103169). We thank Dr. Hiromu Sakurai for his advice on a suitable solvent and buffer solution for electrospraying the vacuum pump oil.

References

[1] R.D. Smith, J.A. Loo, C.G. Edmonds, C.J. Barinaga, H.R. Udseth, Anal. Chem. 62 (1990) 882.
[2] S.A. Shaffer, K. Tang, G.A. Anderson, D.C. Prior, H.R. Udseth, R.D. Smith, Rapid Comm. Mass Spectrom. 11 (1997) 1813.
[3] A.W. Colburn, A.E. Giannakopulos, P.J. Derrick, Eur. J. Mass Spectrom. 10 (2004) 149.
[4] S.A. Shaffer, D.C. Prior, G.A. Anderson, H.R. Udseth, R.D. Smith, Anal. Chem. 70 (1998) 4111.
[5] S.A. Shaffer, A. Tolmachev, D.C. Prior, G.A. Anderson, H.R. Udseth, R.D. Smith, Anal. Chem. 71 (1999) 2957.
[6] K. Tang, A.A. Shvartsburg, H.-N. Lee, D.C. Prior, M.A. Buschbach, F. Li, A.V. Tolmachev, G.A. Anderson, R.D. Smith, Anal. Chem. 77 (2005) 3330.
[7] T. Kim, K. Tang, H.R. Udseth, R.D. Smith, Anal. Chem. 73 (2001) 4162.
[8] A.V. Tolmachev, T. Kim, H.R. Udseth, R.D. Smith, T.H. Bailey, J.H. Futrell, Int. J. Mass Spectrom. 203 (2000) 31.
[9] P. Liu, P.J. Ziemann, D.B. Kittelson, P.H. McMurry, Aerosol Sci. Technol. 22 (1995) 293.
[10] P. Liu, P.J. Ziemann, D.B. Kittelson, P.H. McMurry, Aerosol Sci. Technol. 22 (1995) 314.
[11] P.J. Ziemann, P. Liu, D.B. Kittelson, P.H. McMurry, J. Aerosol Sci. 26 (1995) 745.
[12] H.J. Tobias, P.M. Kooiman, K.S. Docherty, P.J. Ziemann, Aerosol Sci. Technol. 33 (2000) 170.
[13] J.T. Jayne, D.C. Leard, X. Zhang, P. Davidovits, K.A. Smith, C.E. Kolb, D.R. Worsnop, Aerosol Sci. Technol. 33 (2000) 49.
[14] J. Schreiner, C. Voigt, K. Mauersburger, P.H. McMurry, P. Ziemann, Aerosol Sci. Technol. 29 (1998) 50.
[15] J. Schreiner, U. Schmid, C. Voigt, K. Mauersberger, Aerosol Sci. Technol. 31 (1999) 373.
[16] Y. Su, M.F. Sipin, H. Furutani, K.A. Prather, Anal. Chem. 76 (2004) 712.
[17] B. Öktem, M.P. Tolocka, M.V. Johnston, Anal. Chem. 76 (2004) 253.
[18] F. Drewnick, S.S. Hings, P. DeCarlo, J.T. Jayne, M. Gonin, K. Fuhrer, S. Weimer, J.L. Jimenez, K.L. Demerjian, S. Borrmann, D.R. Worsnop, Aerosol Sci. Technol. 39 (2005) 637.
[19] A. Zelenyuk, D. Imre, Aerosol Sci. Technol. 39 (2005) 554.
[20] M. Svane, M. Hagström, J.B.C. Pettersson, Aerosol Sci. Technol. 38 (2004) 655.
[21] X. Wang, P.H. McMurry, Aerosol Sci. Technol. 40 (2006) 320.
[22] X. Wang, F.E. Kruis, P.H. McMurry, Aerosol Sci. Technol. 39 (2005) 611.
[23] X. Wang, A. Gidwani, S.L. Girshick, P.H. McMurry, Aerosol Sci. Technol. 39 (2005) 624.
[24] D.-R. Chen, D.Y.H. Pui, J. Nanoparticle Res. 1 (1999) 115.
[25] D.-R. Chen, D.Y.H. Pui, D. Hummes, H. Fissan, F. Quant, G. Sem, J. Aerosol Sci. 29 (1998) 497.
[26] E.O. Knutson, K.T. Whitby, J. Aerosol Sci. 6 (1975) 443.
[27] K.S. Seol, Y. Tsutatani, R.P. Camata, J. Yabumoto, S. Isomura, Y. Okada, K. Okuyama, K. Takeuchi, J. Aerosol Sci. 31 (2000) 1389.
[28] D.J. Rader, P.H. McMurry, J. Aerosol Sci. 17 (1986) 771.
[29] H.G. Scheibel, J. Porstendörfer, J. Aerosol Sci. 14 (1983) 113.
[30] H. Bartz, H. Fissan, B.Y.H. Liu, Aerosol Sci. Technol. 6 (1987) 163.
[31] D.-R. Chen, D.Y.H. Pui, S.L. Kaufman, J. Aerosol Sci. 26 (1995) 963.
[32] TSI, Model 3480 Electrospray Aerosol Generator Instruction Manual, TSI Inc., St. Paul, 2003.
[33] S.L. Kaufman, J.W. Skogen, F.D. Dorman, F. Zarrin, K.C. Lewis, Anal. Chem. 68 (1996) 1895.
[34] D.-R. Chen, D.Y.H. Pui, Aerosol Sci. Technol. 27 (1997) 367.
[35] T. Myojo, M. Takaya, M. Ono-Ogasawara, Aerosol Sci. Technol. 36 (2002) 76.
[36] W. Li, D.-R. Chen, Aerosol Sci. Technol. 39 (2005) 931.
[37] G. Bacher, W.W. Szymanski, S.L. Kaufman, P. Zöllner, D. Blaas, G. Allmaier, J. Mass Spectrom. 36 (2001) 1038.
[38] J. Fernández de la Mora, L. de Juan, K. Liedtke, A. Schimidt-Ott, J. Aerosol Sci. 34 (2003) 79.
[39] H. Fischer, I. Polikarpov, A.F. Craievich, Protein Sci. 13 (2004) 2825.
[40] M.L. Quillin, B.W. Matthews, Acta Crystallogr. Sect. D 56 (2000) 791.
[41] K.M. Andersson, S. Hovmoller, Acta Crystallogr. Sect. D 56 (2000) 789.
[42] J. Fernández de la Mora, Anal. Chim. Acta 406 (2000) 93.
[43] J.A. Huffman, J.T. Jayne, F. Drewnick, A.C. Aiken, T. Onasch, D.R. Worsnop, J.L. Jimenez, Aerosol Sci. Technol. 39 (2005) 1143.